INERTIAL MEASUREMENT UNIT CALIBRATION PLATFORM

John J. Hall
Robert L. Williams II
Frank van Graas
Ohio University
Athens, OH 45701

Proceedings of the Sixth Conference on Applied Mechanisms and Robotics
Cincinnati OH, December 12-15, 1999

Contact author information:
Robert L. Williams II
Assistant Professor
Department of Mechanical Engineering
257 Stocker Center
Ohio University
Athens, OH 45701-2979
phone: (740) 593 - 1096
fax: (740) 593 - 0476
email: bobw@bobcat.ent.ohiou.edu
URL: http://www.ent.ohiou.edu/~bobw

Inertial Measurement Unit Calibration Platform

John J. Hall and Robert L. Williams II
Department of Mechanical Engineering, bobw@bobcat.ent.ohiou.edu
Frank van Graas
Avionics Engineering Center
Ohio University

ABSTRACT

The Department of Mechanical Engineering and Avionics Engineering Center at Ohio University are developing an electromechanical system for the calibration of an inertial measurement unit (IMU) using global positioning system (GPS) antennas. The GPS antennas and IMU are mounted to a common platform to be oriented in the angular roll, pitch, and yaw motions. Vertical motion is also included to test the systems in a vibrational manner. A four-dof system based on the parallel Carpal Wrist is under development for this task. High-accuracy positioning is not required since the GPS technology provides absolute positioning.

1. INTRODUCTION

There is a need for fast and accurate calibration of manufactured inertial measurement units (IMUs) for use in aircraft navigation. Current machines that perform this task are expensive. This paper presents an alternate calibration system based on variable-geometry truss (VGT) technology.

VGTs are in-parallel-actuated trusses wherein certain key members are replaced with linear actuators. VGTs have a high force-to-weight ratio and are quite stiff compared to serial manipulators. The double octahedral VGT (DOVGT) shown in Fig. 1 was developed at NASA Langley Research Center (Rhodes and Mikulas, 1985) for use as an erectable space station module. The DOVGT has three degrees-of-freedom (dof), with three linear actuators in the mid-plane. DOVGT kinematics solutions were first presented by Padmanabhan, et al. (1992a) and also by Williams (1994). This device was proposed as a robotic joint in a long-reach hybrid serial/parallel manipulator for space and nuclear waste operations (Hughes, et al., 1991, Salerno and Reinholtz, 1994). Williams and Hexter (1998) present a study of optimal design parameters for maximum DOVGT kinematic range of motion.

Figure 1. Double-Octahedral VGT

In his dissertation, Salerno first presented that the kinematics and passive joint design for the DOVGT are significantly simplified if the three linear actuators are mounted to the ground link, directly actuating the three lower DOVGT face angles, see Fig. 2. This led to a patent for an improved DOVGT (Canfield, et al., 1997). The Jacobian matrix and singularity analysis for this Carpal Wrist are presented by Canfield, et al. (1996).

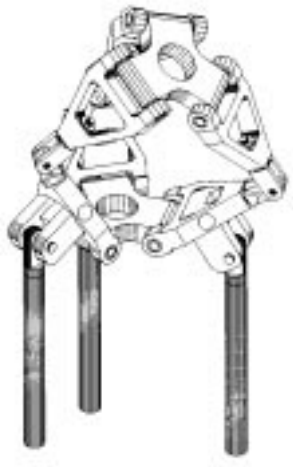

Figure 2. Virginia Tech Carpal Wrist

The IMU calibration platform in this paper is based on the Carpal Wrist device. The pitch and roll motions are provided by coordinated motion of the three linear actuators. The third freedom resulting from these three actuators is the accordion-like translational extension of the platform, used for vertical vibration testing. The yaw rotational freedom is unlimited and provided by a turntable which rotates the entire Carpal Wrist/motion platform mechanism. This paper describes the design, kinematics, construction, and control of this device for avionics applications.

2. THE DESIGN PROBLEM

The Ohio University Avionics Department requested the design and construction of a motion platform. The platform needs to provide pitch, roll and yaw motions for a specific arrangement of four GPS antennas and one multi-axis inertial measurement unit (IMU). The pitch and roll motions are to reach $\pm 45^{\circ}$. The yaw or heading change is to be continuous and bi-directional. The angular rates should achieve approximately π *rad*/*s*. The GPS antennas must be held one meter apart in a cross pattern with the IMU mounted in the center. This cross pattern is representative of the wings and fuselage of an airplane. The GPS antennas and the IMU must be connected to a data collection board for calibration.

This motion platform was built for the primary purpose of calibrating the multi-axis IMU with the GPS antennas. During motion, the data from the GPS antennas in combination with the signals from the IMU can be used to develop specific calibration functions for each unique IMU mounted to the platform. Calibrated IMUs can then be used for on-board aircraft navigation for sensing angular aircraft motion.

Figure 3 presents the detailed CAD design for this IMU calibration platform. The moving cross on top shows the four GPS antennas mounted on the tips and the cubical IMU mounted in the center. The Carpal Wrist is evident in the middle portion, with three linear actuators. A turntable rotates the entire assembly above for the yaw freedom. The remaining structure is the fixed base.

The next section presents a kinematics overview before the detailed design and control description.

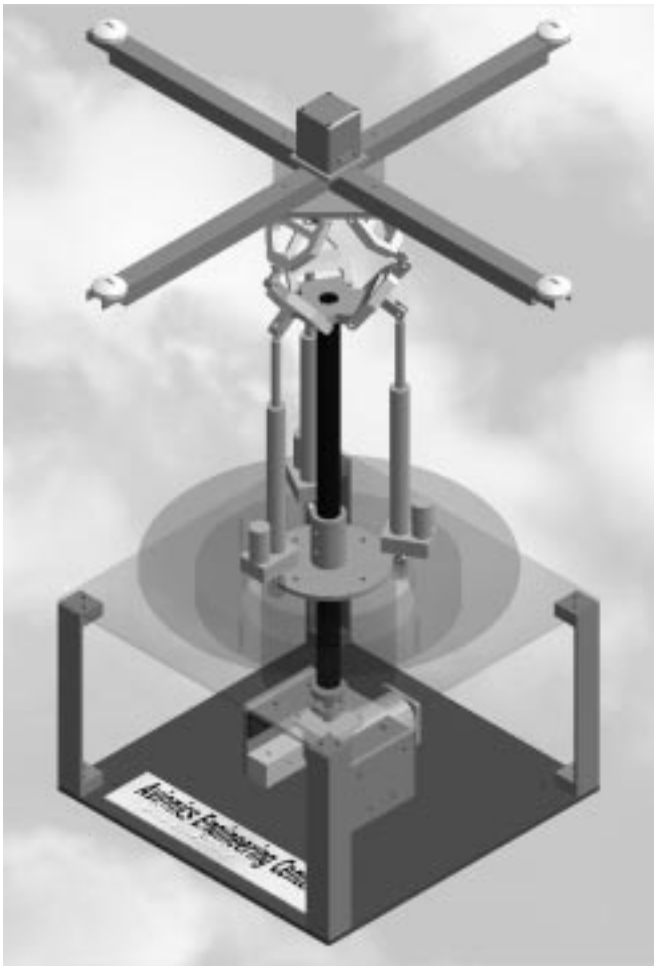

Figure 3. IMU Calibration Platform Design

3. KINEMATICS

Inverse pose kinematics (given the Cartesian values, calculate the leg lengths L_1, L_2, and L_3) is required for control of the Fig. 3 concept, and forward pose kinematics (given the leg lengths, calculate the Cartesian values) is useful for motion simulation. These solutions were first presented by Virginia Tech (Padmanabhan, et al., 1992b). In that work, the DOVGT of Fig. 1 was represented as a virtual extensible gimbal. Figure 4 shows the actual DOVGT the and virtual extensible gimbal kinematic diagrams. The Cartesian values are gimbal angles α and β, and gimbal extension r.

Williams (1994) presents a complete summary of the DOVGT kinematics. He defines three separate problems for the forward and inverse pose kinematics, shown in Fig. 5. Figure 6 shows the definition for DOVGT face angles θ_1, θ_2 and θ_3, for

the lower octahedron. By symmetry, the face angles of the upper octahedron are the same. As shown in Fig. 4, $\hat{n}$ is the unit pointing direction of the normal to the moving platform.

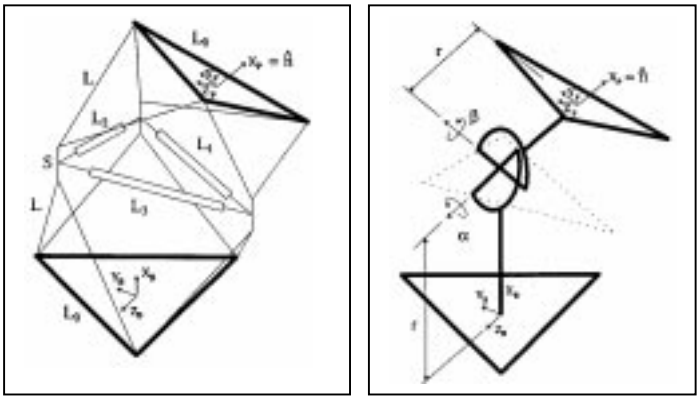

Figure 4. DOVGT and Extensible Gimbal Diagrams

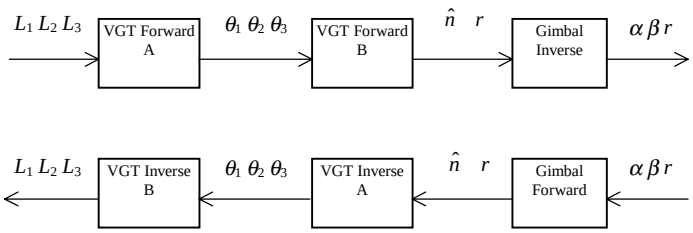

Figure 5. DOVGT Pose Kinematics Problems

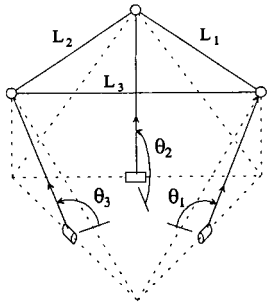

Figure 6. Lower Octahedron Face Angles

The only differences in the pose kinematics between the DOVGT and the Carpal Wrist are in VGT Forward A and VGT Inverse B. The VGT Forward A and VGT Inverse B solutions are replaced with Carpal Forward A and Carpal Inverse B, which are now presented. Refer to Williams (1994) for complete details on the other blocks in Fig. 5. In the Carpal Wrist, each linear actuator L_1, L_2 and L_3 directly controls each angle θ_1, θ_2 and θ_3. Figure 7 shows the variables used for each Carpal Wrist actuator. L_i represents the linear actuator length. G is a fixed vector. R is a fixed-length vector with variable angle ϕ_{Ri}. The angle ϕ_0 is fixed.

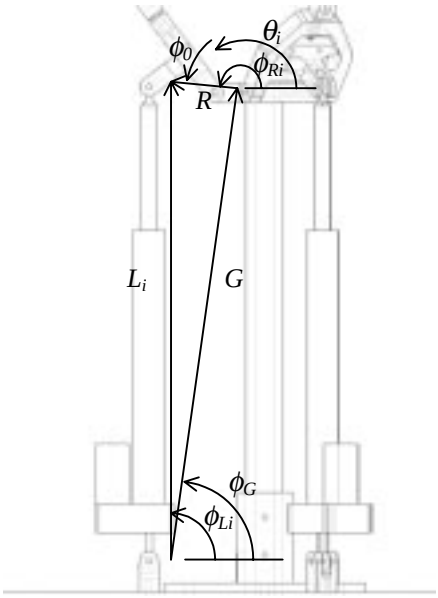

Figure 7. Variables for Carpal Kinematics

By symmetry in design, G, ϕ_G, the length of R, and ϕ_0 are identical for all three legs.

3.1 Carpal Forward A

The Carpal Forward A problem is stated: Given L_i, find θ_i, independently for i = 1,2,3. The following vector loop-closure equation is written from Fig. 7.

$$\vec{L} = \vec{G} + \vec{R} \tag{1}$$

The Cartesian components equations of (1) are:

$$\begin{aligned} \left|\vec{L}\right|\cos\phi_{Li} &= \left|\vec{G}\right|\cos\phi_G + \left|\vec{R}\right|\cos\phi_{Ri} \\ \left|\vec{L}\right|\sin\phi_{Li} &= \left|\vec{G}\right|\sin\phi_G + \left|\vec{R}\right|\sin\phi_{Ri} \end{aligned} \tag{2}$$

Equations (2) are squared and added to eliminate ϕ_{Li}:

$$L_i^2 = G^2 + R^2 + 2GR\left(c\phi_G c\phi_{Ri} + s\phi_G s\phi_{Ri}\right) \tag{3}$$

Equation (3) is a transcendental equation in one unknown ϕ_{Ri} (which is related to unknown θ_i), rewritten as:

$$\begin{aligned} A\cos\phi_{Ri} + B\sin\phi_{Ri} + C &= 0 \\ A &= 2GR\cos\phi_G \\ B &= 2GR\sin\phi_G \\ C &= G^2 + R^2 - L_i^2 \end{aligned} \tag{4}$$

Equation (4) is solved using the well-known tangent half-angle substitution, resulting in two solutions for ϕ_{Ri}. Only one solution makes sense for the hardware. Finally, the solution is $\theta_i = \phi_{Ri} - \phi_0$. This solution is far simpler than VGT Forward A since the three legs are decoupled.

3.2 Carpal Inverse B

The Carpal Inverse B problem is stated: Given θ_i, find L_i, independently for i = 1,2,3. Vector loop-closure equation (1) again applies. First, calculate $\phi_{Ri} = \theta_i + \phi_0$. Then evaluate the right-hand sides of (2); name these components L_{ix} and L_{iy}. The solution is then:

$$L_i = \pm\sqrt{L_{ix}^2 + L_{iy}^2} \qquad i = 1,2,3 \qquad (5)$$

Equation 2 gives us the necessary actuator length L_i for a given angle θ_i. We choose only positive length in (5).

4. HARDWARE DESIGN

The Carpal Wrist was designed for maximum pitch and roll angular displacements. The design parameters for optimal pitch and roll were taken from Williams and Hexter (1998), for the DOVGT configuration in Figs. 1 and 4 (with midplane-mounted actuators). *S* is the offset at the passive joint connection of the longerons and linear actuators. Williams and Hexter concluded that this term had little effect on the maximum obtainable pitch and roll. The range of values used in their optimization included the case *S*=0 which is kinematically similar to the Carpal Wrist (with base-mounted actuators). The optimal ratio of L_0/L = 1.14 is the key result. L_0 is the base and moving equilateral triangle side and *L* is the length of all longeron members.

L_0 = 7" for the Carpal Wrist in Fig. 3. The optimal ratio then yields 7"/1.14 or 6.14" for *L*. As seen in Figs. 8a and 8b, the Carpal Wrist link designs are based on these numbers. These links were designed using CAD and cut with a CNC mill.

The hardware design shown in Fig. 3 utilizes a Carpal Wrist mounted to a turntable. The Carpal Wrist provides pitch, roll and vertical translation. The turntable provides the continuous bi-directional rotation for yaw (heading angle). The turntable was designed to be rigid to provide a solid base for the moving platform. The calibration data collection board is mounted on top of the turntable and is directly connected to the GPS antennas and the IMU. The data collection board communicates with the controlling computer via a slip-ring connection under the turntable.

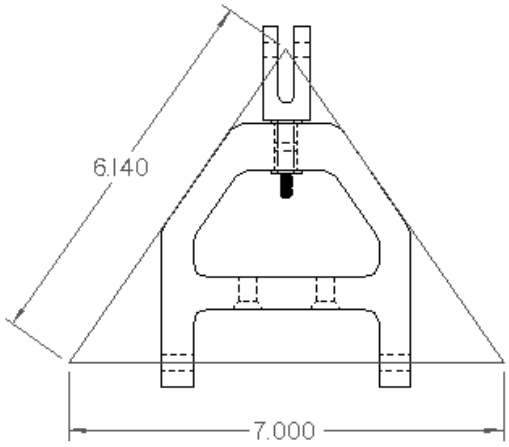

Figure 8a. Carpal Wrist Longeron Link

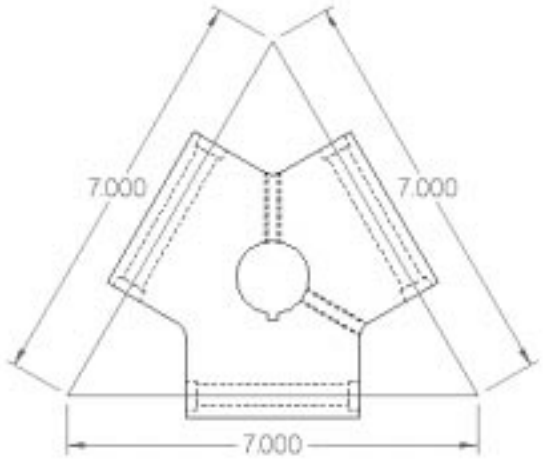

Figure 8b. Carpal Wrist Base Plate

The system mechatronic control elements are shown in Fig. 9. Three acme-screw linear actuators powered via DC servomotors through a gearbox, as seen in Fig. 3, provide the three length inputs to the Carpal Wrist. The command and feedback signals for these actuators are carried back and forth through the slip-ring. The feedback for the linear actuators comes from a built-in potentiometer (linear variable resistor). A brushless DC servomotor with a 22:1

right-angle planetary gear head drives the turntable. A 1000 count encoder with quadrature provides the turntable feedback. This provides 88,000 pulses per revolution of the turntable.

A Multi-Q control board from Quanser Corporation provides the control of the leg and turntable servomotors. This system enables closed-loop hardware control in real-time from Matlab's Simulink environment. The Quanser Multi-Q board requires Matlab with Simulink and the Real Time Workshop. It also requires that Visual C++ be installed. This all works together with the Wincon software provided by Quanser. Models built in Simulink can be readily compiled and run for real-time control.

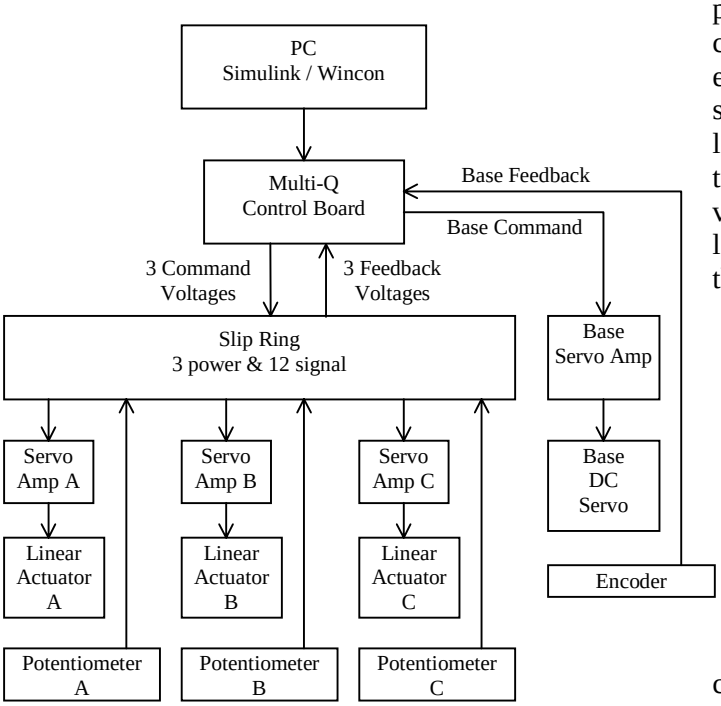

Figure 9. Calibration Platform Mechatronic Design

5. CONTROL ARCHITECTURE

Figure 9 shows the hardware control architecture. The hardware is controlled primarily in inverse pose mode: Given the desired Cartesian pitch, roll, and extension values α, β, and r, and the yaw angle, calculate active prismatic actuator lengths L_1, L_2, and L_3, and the turntable angle. This inverse pose solution was discussed and adapted to the Carpal Wrist from the DOVGT in Section 3. The system may also be controlled in rate mode, either by inputting a time-based series of inverse pose inputs, or by implementing resolved-rate control using the Jacobian matrix as presented in Canfield, et al. (1996).

Regardless of the Cartesian control method, low-level joint control of the turntable angle and the three linear actuator lengths is required. The closed-loop feedback joint control diagram is shown in Fig. 10 for one of the linear actuators (the turntable angle diagram is similar).

In Fig. 10, L_C is the commanded leg length for prismatic actuator *i*. L_E is the length error. V is the voltage to be applied to the acme-screw DC servomotor, calculated by the proportional-integral-derivative (PID) control law. L_A is the actual prismatic actuator length resulting from this voltage command (and the ensuing dynamic response of the entire system, i.e. four actuators operating simultaneously). L_S is the sensed value of this actual length, as read by the potentiometer feedback. The turntable angle block diagram is very similar: The variables are turntable angle instead of actuator length, and the feedback sensor is the encoder rather than a potentiometer.

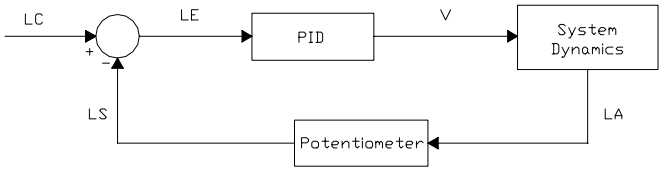

Figure 10. Actuator Length Control Block Diagram

In this manner we achieve coordinated Cartesian control of the calibration platform via linearized independent (but simultaneous) linear actuator and turntable angle joint control. We have not derived the system dynamics block in Fig. 10; in fact, the Simulink diagram implementation of Fig. 10 is open at these blocks (the real-world hardware and sensors close the loop). Rather, the PID gains have been determined experimentally by setting the proportional gain first (starting with low values and working up!) and adding the integral and derivative terms as needed (again, starting with low values). We use the Simulink PID block (with approximate derivative to minimize the problems with numerical differentiation). Initially the PID design was performed for individual actuators on the benchtop. Using these gains as a starting point, the next step is to perform the PID design for each actuator within

the context of the coupled system dynamics. General control design specifications are smooth motion, low overshoot, plus fast rising and settling times.

6. PRELIMINARY RESULTS

The calibration platform system mechatronic design has been completed and the system has been constructed at Ohio University, as shown in Fig. 11. Preliminary PID controller design has been accomplished for each actuator on the benchtop. Sample actuator control results are given in this section.

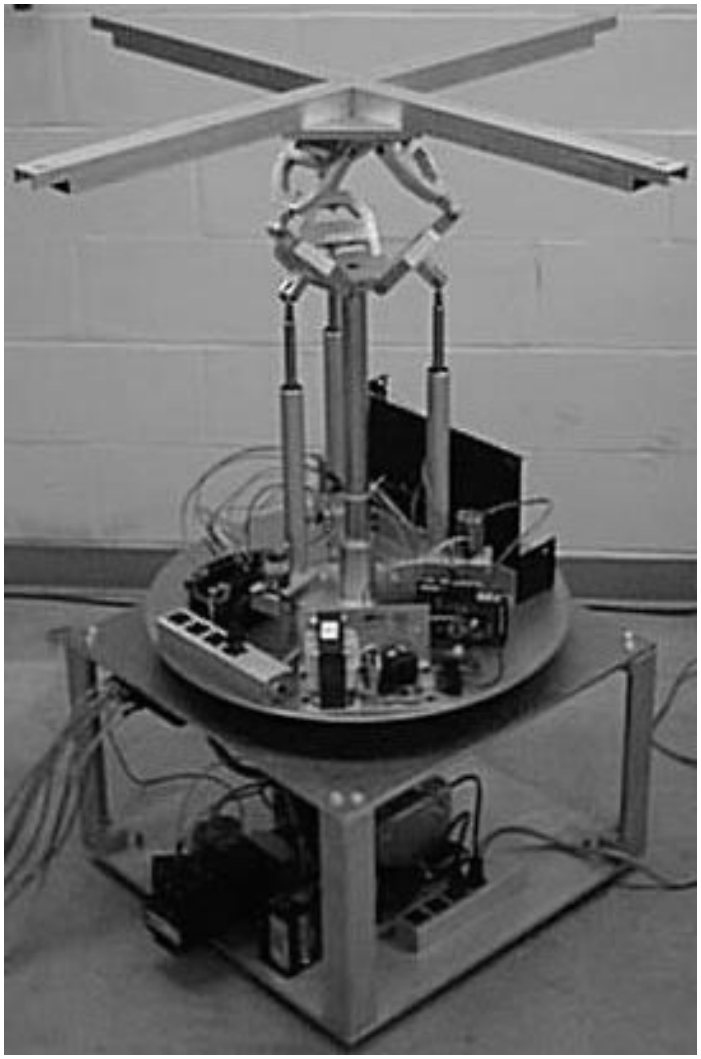

Figure 11. Calibration Platform Hardware

Figure 12 shows a sample result for hardware linear actuator control on the benchtop (not within the coupled dynamic system). Independent control of all three legs is similar, so only one result is shown. For this case, the actuator length was commanded from the minimum extent to a displacement of 2". As shown in Fig. 12, this command (dotted line) is a ramped step input; the slope shown is higher than it could be for the coupled, fully loaded system. The actual control results (solid line) follow the input command well, but a steady-state error is evident in Fig. 12. To improve positioning accuracy, a zero-backlash ball-screw actuator with encoder feedback could replace the acme-screw with potentiometer feedback. However, both components would be more expensive. The ball-screw can be back-driven and thus would collapse when power is lost. Also, the encoder would require double the number of channels in the slip-ring. One strength of the proposed system is that the GPS technology provides the absolute positioning accuracy for the IMU calibration, so the Carpal Wrist positioning accuracy may be lower.

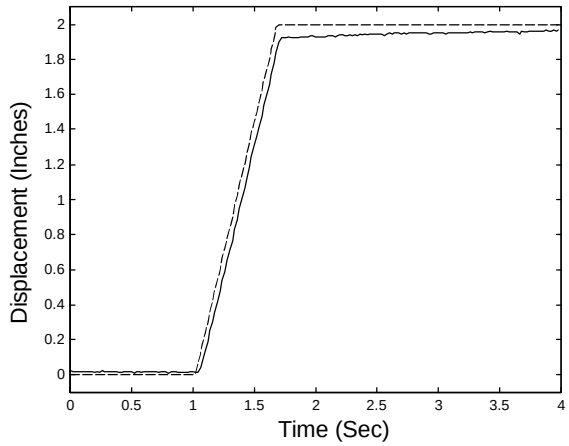

Figure 12. Actuator Length Control

Figure 13 shows a sample result for hardware turntable angle control. For this result, the commanded turntable angle was two revolutions. Again, the commanded ramped step is dashed, while the actual angle feedback is the solid line. Figure 13 demonstrates that the turntable angle performance is very good. There is zero steady-state error and the actual results have the commanded turntable rate of π *rad/s*.

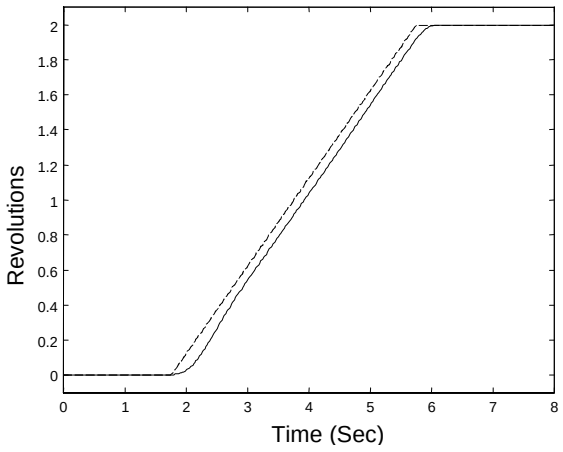

Figure 13. Turntable Angle Control

The next steps in calibration platform controls implementation are: 1) Detailed, effective PID design for control of each of the four joints within the coupled dynamic system; 2) Cartesian motion planning for the calibration and other tasks; and 3) Development of an intuitive user interface for system operation.

7. CONCLUSION

This paper has presented a new electromechanical system for automated calibration of inertial measurement units (IMUs) using global positioning system (GPS) antennas. The four-dof system consists of an in-parallel-actuated Carpal Wrist that rotates on a turntable. The Carpal Wrist provides pitch, roll, and vertical displacement, while the turntable provides the yaw freedom necessary for general calibration motions. A prototype system has been designed and constructed at Ohio University, and preliminary controller implementation has been accomplished. In the future we will complete controls implementation for the calibration task and explore other tasks which could be performed by this machine. One benefit of this calibration system over existing alternatives is that the robot system need not provide high-accuracy positioning capability since the GPS technology provides absolute positioning accuracy for the IMU calibration process.

REFERENCES

S.L. Canfield, C.F. Reinholtz, R.J. Salerno, and A.J. Ganino, 1997, *"Spatial, Parallel-Architecture Robotic Carpal Wrist"*, U.S. Patent 5,699,695.

S.L. Canfield, A.J. Ganino, R.J. Salerno, and C.F. Reinholtz, 1996, *"Singularity and Dexterity Analysis of the Carpal Wrist"*, ASME Design Technical Conferences, 24th Biennial Mechanisms Conference, Irvine, CA.

P.C. Hughes, W.G. Sincarsin, and K.A. Carroll, 1991, *"Trussarm: A Variable Geometry Truss Manipulator"*, **Journal of Intelligent Materials, Systems, and Structures**, 2: 148-161.

B. Padmanabhan, V. Arun, and C.F. Reinholtz, 1992a, *"Closed-Form Inverse Kinematic Analysis of Variable-Geometry Truss Manipulators"*, **Journal of Mechanical Design**, 114: 438-443.

B. Padmanabhan, P. Tidwell, R.J. Salerno, and C.F. Reinholtz, 1992b, *"VGT-Based Gimbals: Practical Construction and General Theory"*, ASME Mechanisms Conference, Phoenix, AZ, DE-Vol 47: 437-443.

M.D. Rhodes and M.M. Mikulas Jr., 1985, *"Deployable Controllable Geometry Truss Beam"*, **NASA Technical Memorandum 86366**, NASA Langley Research Center, Hampton, VA.

R.J. Salerno, 1993, *"Positional Control Strategies for a Modular, Long-Reach, Truss-Type Manipulator"*, Ph.D. Dissertation, Virginia Polytechnic University and State University, Blacksburg, VA.

R.J. Salerno and C.F. Reinholtz, 1994, *"A Modular, Long-Reach, Truss-Type Manipulator for Waste Storage tank Remediation"*, ASME Mechanisms Conference, Minneapolis, MN, DE-Vol. 72: 153-159.

R.L. Williams II, 1994, *"Kinematic Modeling of a Double Octahedral Variable Geometry Truss (VGT) as an Extensible Gimbal"*, **NASA Technical Memorandum 109127**, NASA Langley Research Center, Hampton, VA.

R.L. Williams II and E.R. Hexter IV, 1998, *"Maximizing Kinematic Motion for a 3-DOF Variable Geometry Truss Module"*, **Journal of Mechanical Design**, 120 (2): 333-336.